Journal Name

ARTICLE

Orientation direction dependency of cavitation in pre-oriented isotactic polypropylene at large strains†

Received 00th January 20xx,
Accepted 00th January 20xx

DOI: 10.1039/x0xx00000x

www.rsc.org/

Ying Lu,[a] Glen Thompson,[b] Dong Lyu,[ac] Philip Caton-Rose,[b] Phil Coates*[b] and Yongfeng Men*[ac]

Orientation direction dependency of whitening activated at large strains was studied using four pre-oriented isotactic polypropylene (iPP) samples with different molecular weights stretched along different directions with respect to the pre-orientation (0°, 45°, and 90°) by means of in-situ wide-, small-, and ultra-small-angle X-ray scattering techniques. A macroscopic fracture of iPP materials was also observed following the stress whitening at large strains. These two associated processes in pre-oriented iPP samples at elevated temperatures were found to be governed by not only the molecular weight of iPP but also the pre-orientation direction. For a certain pre-orientation direction of iPP, both the critical stress of cavitation induced-whitening and failure stress increased with increasing molecular weight. For one given molecular weight, the pre-oriented iPP showed the smallest critical stress for whitening and failure stress along pre-orientation direction (0°) while the samples displayed larger values for the same behaviors when stretched along 45° or 90° with respect to pre-orientation direction. Such behavior suggested that oriented amorphous networks, with different mechanical strength, can be generated during the second deformation processes in these pre-oriented iPP samples. The evolution of inter-fibrillar tie chains in highly oriented amorphous networks was considered as the main factor controlling the response of the inner network to the external stress since the cavitation-induced whitening activated at large strains was caused by the failure of load bearing inter-fibrillar tie chains in the oriented amorphous network.

1 Introduction

Isotactic polypropylene (iPP) is of great industrial interest and has been used in a plethora of applications, e.g., packaging, plastic pipes, automotive and aircraft products, due to its outstanding processability, excellent chemical resistance, low density and cheap cost.[1] However, in spite of these advantages, application of iPP as an engineering plastic is still restricted because of relatively poor toughness at low temperatures or high strain rates. Efficient approaches to improve its ultimate property of toughness have focused on inducing different crystalline modifications such as the α crystal form,[2-6] the mesophase,[7, 8] and the β phase of low crystallinity.[9] These methods offer iPP samples with enhanced toughness and ductility, however, at the sacrifice of the material's modulus and tensile strength.[4] Recently, overstretched high density polyethylene (HDPE) drawn perpendicular and 45° with respect to the pre-orientation direction showed increases in maximum achievable strain and stress several times higher than the isotropic form before macroscopic failure.[10] The HDPE featured with a notable reinforcement and distinct advantage of ductility clearly can be successfully achieved using drawing overstretched HDPE samples.[10] Therefore, this finding could be served as a possible route to produce high performance polypropylene products in the solid state.

The efficient processes for inducing highly oriented iPP are generally associated with shearing,[11-15] injection,[16-20] as well as die drawing.[21-25] The former two normally can lead to the side product of β crystallites which weakens the stiffness of material.[2-6] In other words, these two methods can create oriented iPP but at the expense of consuming the material's modulus and tensile strength,[4] which is not a satisfying consequence for commercial and scientific fields. The solid processing of the die drawing process, is described as confined stretching.[26] The main deformation region of die drawing is the inside of a die and the properties of materials generally keep constant after out of the die, providing "steady state" stretching conditions for materials.[27] Meanwhile, such processing usually can bring out the polymer with suitably strain hardening and process variables with appropriate values.[28, 29] Stretching iPP at high temperatures always leads to only α modification. Therefore, the die drawing process seems to be an efficient approach to attain oriented α modification iPP with ultrahigh modulus and an even distribution deformation state at high deformation temperatures.

[a] State Key Laboratory of Polymer Physics and Chemistry, Changchun Institute of Applied Chemistry, Chinese Academy of Sciences, Renmin Street 5625, 130022 Changchun, P. R. China. E-mail: men@ciac.ac.cn
[b] School of Engineering, Design and Technology, University of Bradford, Bradford BD7 1DP, U. K. E-mail: Coates@bradford.ac.uk
[c] University of Science and Technology of China, Hefei 230026, P. R. China
†Electronic Supplementary Information (ESI) available: details of measuring the width of tensile bar and fraction of original crystallites. See DOI: 10.1039/x0xx00000x

A cavitation process trigged at large strains of iPP has been established lately,[30] which significantly differs from the cavitation activated around the yield point.[31-35] The former one is proposed as the creation of cavities within the highly oriented samples, during which a critical stress triggering the stress whitening is needed. That critical stress is found to depend only on molecular weight and irrespective of stretching temperature, attributing this stress whitening under large strains to be interpreted as a consequence of inter-fibrillar tie chains breaking within the highly oriented amorphous network.[30] The case of stress whitening at small strains is defined as cavities generated at the lamellae scale, which can be basically influenced by the preparation methods of the material as well as testing conditions.[36-40] Meanwhile, the appearance of cavitation around the yield point aids the materials to be stretched to a large extension without breaking. However, a fragmentation of materials usually follows the stress whitening presented at large strains. Thus, the failure mechanism of iPP upon stretching somehow appears to be linked with the occurrence of cavities activated at large strains.

In current work, we employed four pre-oriented iPP samples with different molecular weights obtained via the die drawing process to investigate the deformation behaviors at high temperatures, attempting to explain the mechanism of microscopic failure and stress whitening occurring in pre-oriented iPP materials at the late deformation stage. In-situ wide-, small-, and ultra-small-angle X-ray scattering (WAXS, SAXS, and USAXS) measurements were used to record the microstructural evolution of iPPs during the deformation process. Both the molecular weight and pre-orientation direction of iPP were considered as factors controlling the stress whitening which appeared at large strains, which then gave rise to macroscopic failure. We hypothesized that the fragmentation of load bearing inter-fibrillar tie chains should be responsible for stress whitening triggered at large strains. This was due to the fact that the number of inter-fibrillar tie chains was the major parameter showing difference in draw iPP samples obtained from different molecular weights and pre-orientation directions. The following macroscopic fracture of iPP after stress whitening at large strains was attributed to be a consequence of a full-scale breakage of oriented amorphous network caused by the generation and growth of cavities.

2 Experimental

2.1 Materials and sample preparation

A series of commercial iPP samples purchased from Aldrich Polymer Products were investigated. Table 1 lists the details of iPP samples. The iPP pellets were first molded in a plate with dimensions of 150 × 150 mm^2 under a hot press at 200 °C for 10 minutes, developing sheets of 1 mm in thickness. Then, these sheets were still kept at 200 °C for 1 minute under the press of 10 MPa. After that, the press was removed to let the molecular chains relax for 5 minutes at 200 °C. Finally, such sheets were quickly quenched into the tank with cold water and stabilized for 20 minutes. The obtained films were transparent due to low crystallinity formed at low crystallization temperature. Rectangular strips with dimensions of 1 × 25 × 150 mm^3 were cut from the quenched sheets using a manual guillotine to create samples suitable for the die drawing tests.

Table 1 The basic physical properties of iPPs used in experiments

Catalog No.	Name	Melt Index	M_w (Kg mol^{-1})	M_n (Kg mol^{-1})	T_m / °C[a]
427896	iPP190K	35	190	50	165
427888	iPP250K	12	250	67	165
427861	iPP340K	4	340	97	165
427853	iPP580K	0.5	580	166	165

[a] Detected by DSC with a heating rate of 10 K/ min.

2.2 Die drawing tests

Fig. 1 schematically shows the die drawing process.[41] A heated polymer billet is drawn through a heated converging die by applying a pulling force on the billet at the exit side of the die. The polymer billet is free to neck down and follows an optimum strain and strain rate path through the die, leaving the die wall at an appropriate point.[41] For pre-heating the polymer billet, an oven is linked to the die supporting this procedure. In order to calculate the true axial draw ratio R_A of the material during the die drawing process, the R_A of rectangular strips is generally defined as[41]

$$R_A = \frac{A_0}{A_f} \quad (1)$$

where A_o and A_f are the initial and final cross-sectional dimensions of product, respectively. The die used in the current work is designed by Professor Coates's lab at the University of Bradford. It is characterized with a die exit width of 25 mm while the die exit thickness adjustable to allow for controlled imposed nominal draw ratio. In terms of our experiments, the dimensions of initial cross-sectional area of iPP was 25 × 1 mm^2 and 0.5 mm was chosen as the exit thickness. Both the temperatures in the oven and die were set at 140 °C during stretching. An initial crosshead speed of 3.6 mm s^{-1} was imposed which then increased to 15.8 mm s^{-1} for the fuller draw. After stretching, the strips were fixed at their two ends for 20 minutes before taking them out of the die and the clamp. The final cross-sectional area of iPP was around 22 × 0.48 mm^2. Therefore, the draw ratio R_A of iPP samples was about 2.27. Macroscopically, no stress whitening was observed during the whole die drawing process.

After the die drawing process, the "dog bone" tensile bars with dimensions of 22 x 5 x 0.48 mm^3 were cut directly from the

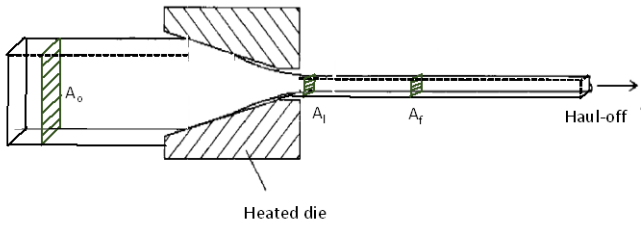

Fig. 1 Schematic diagram of the die drawing process.

die drawn iPP samples with the aid of a punch at one of three angles, 0°, 45°, and 90°, with respect to the original stretching direction. Uniaxial tensile deformation was carried out using a portable tensile testing machine (TST350, Linkam, UK) with a clamping distance of 10 mm. This machine is also equipped with a Linkam heating system (made of silver), supporting the temperature test from room temperature to 350 °C. The variation of cross-head speed of this machine is from 1 to 1000 μm s^{-1}. We employed a stepwise tension at a constant cross-head speed of 20 μm s^{-1} (equal to an initial strain rate of 0.0013 s^{-1}) for stretching iPP samples at deformation temperatures of 115, 125, and 135 °C. During stretching, the tensile bar was directly contacted with the silver block to ensure the constant stretching temperature in the optical observation area of sample.

2.3 method for calculating true strain during stretching

For the purpose of measuring the strain of the deformed area, optical images of the samples were taken during stretching processes. The deformation of the materials was found to be inhomogeneous, ascribed by the appearance of a neck, so that the engineering strain was no longer suitable for describing the deformation process. Clearly, the true strain is needed to express the local strain of materials during the stretching process. Thus, the Hencky strain ε_H is used as a basic quantity of the true strain, which is defined as

$$\varepsilon_H = 2\ln\frac{b_0}{b} \quad (2)$$

where b_0 and b are the widths of the initial and instant width located at certain spots on the samples, respectively. The measurements of b_0 and b are provided in the Fig. S1 of ESI. For calculating the true stress σ at one certain strain, the equation below is employed:

$$\sigma = \frac{F}{s_0}\left(\frac{b_0}{b}\right)^2 \quad (3)$$

where F and s_0 are the instant load on sample during stretching and the initial cross-section area (width x thickness) of sample, respectively.

2.4 Ultra-small angle X-ray scattering (USAXS)

For the sake of exploring the stress whitening presented at large strains, in-situ ultra-small angle X-ray scattering (USAXS) experiments were conducted with a modified Xeuss system of Xenocs, France, at a sample-to-detector distance of 6558 mm providing effective scattering vector q ($q = (4\pi\sin\theta)/\lambda$, where 2θ is the scattering angle and λ the wavelength of the X-ray.) range from 0.022 to 0.24 nm^{-1}. A multilayer focused Cu K_α X-ray source (GeniX3D Cu ULD, Xenocs SA, France, λ= 0.154 nm) and scatterless collimating slits were used during the experiments. The size of the primary X-ray beam at the sample position was 0.8 × 0.8 mm^2. USAXS images were recorded with a Pilatus 100K detector of Dectris, Swiss (487 pixels × 197 pixels, pixel size= 172 μm). The exposure time for one USAXS pattern was set as 300 seconds.

2.5 Wide angle X-ray scattering (WAXS)

Additionally, in-situ wide angle X-ray scattering (WAXS) experiments were performed at a custom-designed micro-focus X-ray beam of Xeuss system of Xenocs, France. The system is equipped with a same X-ray generator as described above but used a strong focusing mirror focuses the X-ray to a spot size of 40 × 60 μm^2 at the sample position. Each WAXS diagram obtained in the center of the sample was collected within half a minute at a sample-to-detector distance of 39 mm through a Pilatus 100K detector of Dectris, Swiss. Moreover, the Hermans formula[42] was applied to calculate the orientation parameter, which is expressed as

$$S_{hkl} = \frac{2<\cos^2\phi_{hkl}>-1}{2} \quad (4)$$

where ϕ_{hkl} denotes the angle between the drawing direction and the normal vector of the lattice plane (*hkl)*. Additionally, orientation parameter $\cos^2\phi_{hkl}$ can be achieved from azimuthal scattering intensity distribution by the following equation

$$\cos^2\phi_{hkl} = \frac{\int_0^{\pi/2} I_{hkl}(\phi)\cos^2\phi\sin\phi d_\phi}{\int_0^{\pi/2} I_{hkl}(\phi)\sin\phi d_\phi} \quad (5)$$

where $I_{hkl}(\phi)$ describes the scattering intensity along the angle ϕ. And ϕ can be obtained by using Polanyi equation[43]

$$\cos\phi_{hkl} = \cos\theta_{hkl}\cos\psi \quad (6)$$

where θ_{hkl} denotes the Bragg scattering angle, ψ is the azimuthal angle along the Debye circle. Generally, for a perfect orientation of the lattice plane with its normal in the plane of equator, the order parameter S is equal to -0.5. For an isotropic sample, the order parameter S is usually presented as 0. Therefore, when the material drawn from the isotropic state to the large strain, the orientation parameter can vary in the range of 0 to -0.5.

2.6 Small angle X-ray scattering (SAXS)

Furthermore, in- situ synchrotron SAXS experiments with a sample-to-detector distance of 1945 mm were carried out at beamline BL16B at SSRF, Shanghai, China, providing the effective scattering vector q range from 0.065 to 1.99 nm^{-1}. The X-ray with a wavelength of 0.124 nm was focused to a spot size of 0.5 × 0.5 mm^2 at the sample position Each SAXS pattern was collected within 80 seconds using a Mar CCD detector (2048 pixels × 2048 pixels, pixel size= 80 μm) which was then background corrected and normalized using the standard procedure. The one dimensional radial scattering intensity distributions were integrated within ± 20° along the normal direction of lamellae on 2D SAXS patterns, and the value of long spacing d_{ac} was calculated by using the Bragg equation

$$d = \frac{2\pi}{q_{max}} \quad (7)$$

the q_{max} represents the maximum q point in the SAXS patterns for the periodic lamellar structure when scanning along certain directions.

3 Results and discussion

Fig. 2 shows the true stress-strain curves of pre-oriented iPP samples with different pre-orientation directions drawn at 115 °C. These curves were obtained through connecting all the true stresses at the corresponding strains in the whole stretching process. A closer inspection of these stress-strain curves at the final stages reveals that the failure stresses of iPP increased with increasing iPP molecular weight for a given pre-orientation direction. Tests also showed larger values in the 45 and 90° pre-oriented samples compared to the 0° pre-oriented one for a given molecular weight iPP. A notable improvement of ductility was observed in the 45 and 90° pre-oriented samples as well. The pre-orientation dependency of failure stress and strain were in agreement with the performance found in overstretched polyethylene.[10] Furthermore, the selected photographs presented in Fig. 2 revealed an ordinary evolution of cavitation at large strains: a sudden localized whitening occurred at a large strain which then propagated to the whole sample with further stretching.[30] In order to understand the appearance of such stress whitening in pre-oriented materials, the corresponding critical stresses of whitening for each specimen are represented by the open circles on the plot. Such values are denoted using the true stresses representing the first occurrence of whitening on the photographs during different deformation processes. These critical stresses showed the similar tendency as shown in fracture stresses, which were related to the iPP molecular weight and pre-orientation direction.

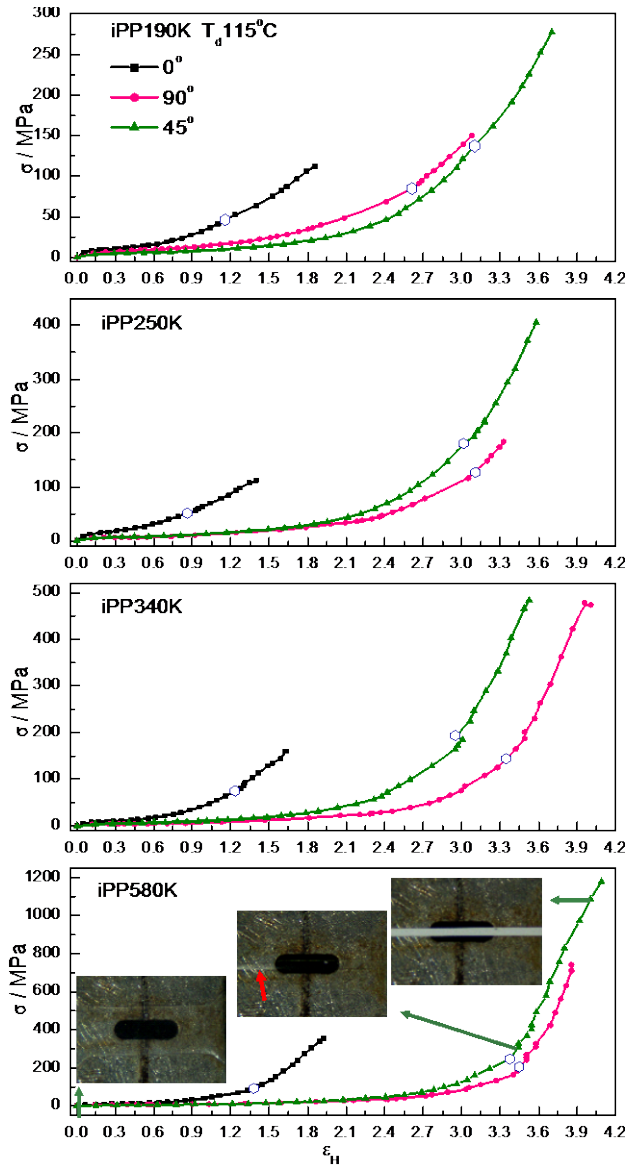

Fig. 2 True stress-strain curves of pre-oriented iPP samples measured at 115 °C. The open circles represent the positions of initial whitening of the samples on the stress–strain curves. (The selected photographs of die drawn iPP580K were also included.)

Fig. 3 gives the further details of critical stresses of whitening at large strains of pre-oriented iPPs deformed at different temperatures. For a certain pre-orientation direction, the lowest molecular weight iPP190K presented the smallest critical stresses of whitening at large strains while the highest molecular weight iPP580K displayed the largest values for this behavior. For example, the critical stresses of whitening were about 45, 50, 75, and 90 MPa in the 0° pre-oriented iPP190K, iPP250K, iPP340K, and iPP580K, respectively. Besides, the critical stresses of whitening for stretching isotropic iPP250K and iPP580K samples have been found around 50 and 90 MPa irrespective of deformation temperatures as shown in our previous work.[30] Here, the same critical stresses of whitening can be observed in the 0° pre-oriented iPP250K and iPP580K samples at all stretching temperatures, indicating that the two-step deformation process has no effect on the critical stresses triggering whitening at large strains. In the case of a certain molecular weight iPP, the previous orientation direction obviously affected the critical stresses of whitening at large strains. For instance, the critical stress for activating this special whitening of the 0° pre-oriented iPP190K only needed to approach 45 MPa while such value increased to 130 MPa for the 45° pre-oriented iPP190K. The situation in the 90° pre-oriented iPP190K was just between the former two cases. The behaviors observed above clearly suggested a distinct difference of critical

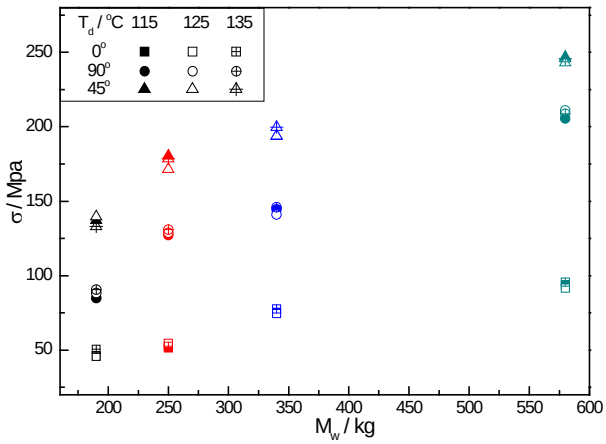

Fig. 3 The critical stresses of initial stress whitening presented in pre-oriented iPPs as a function of molecular weight at different deformation temperatures. (Symbols: the square, circle, and triangle points represent the 0°, 90°, and 45° pre-oriented samples, and the solid, hollow, cross points represent stretching temperatures of 115, 125, and 135 °C, respectively.)

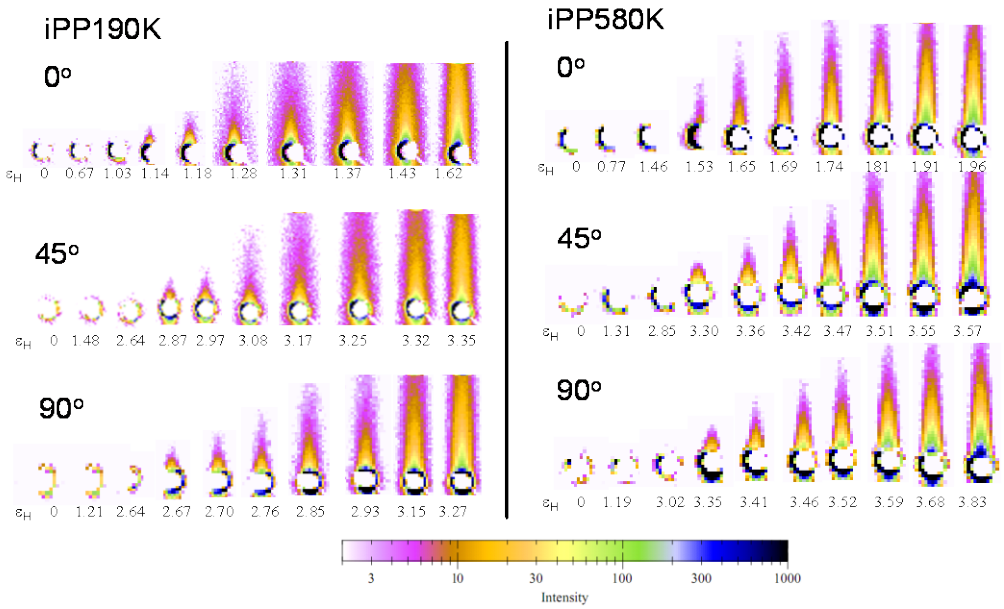

Fig. 4 Selected USAXS patterns of die drawn iPP190K (left) and iPP580K (right) deformed at 115 °C taken at different strains as indicated on the graph. (Deformation direction: horizontal)

stresses of whitening presented in different molecular weight iPPs as well as previous orientation directions.[44]

In order to understand these performances, attention should be focused on the essential cause of stress whitening initiated at larger strains which has been identified as a consequence of the fragmentation of the inter-fibrillar tie chains in highly oriented amorphous network.[30] Generally, higher molecular weight iPP sample possesses a larger number of entanglements and tie chains which can induce a larger number of load bearing inter-fibrillar tie chains,[45] so that it demands larger critical stresses to break the oriented amorphous network. Hence, it was easy to understand one particular pre-oriented iPP samples exhibited molecular weight dependency of stress whitening at large strains. However, a further analysis should be implemented to understand the influence of pre-orientation direction of molecular chains on the occurrence of stress whitening at large strains. The main analysis will be concentrated on this topic in the following sections.

Fig. 4 collects the selected USAXS patterns of pre-oriented iPP190K and iPP580K samples during stretching. At the beginning of tensile tests, no scattering signal could be observed in such patterns whereas an appearance of very intense scattering streaks perpendicular to the stretching direction abruptly came into sight at a certain strain in all iPPs. These scattering streaks could only be ascribed to elongated cavities since the scattering from crystalline lamellar stacks in the iPPs exceeded the limited scattering vector q of USAXS equipment.[30] In order to describe the intensity of cavities produced in pre-oriented iPP samples, the corresponding total scattering intensities of pre-oriented iPP samples during stretching are depicted in Fig. 5 through integrating the USAXS patterns. Such total integrated intensity Q is defined as[46]

$$Q = (c_{e,c} - c_{e,m})^2 \phi_c (1 - \phi_c) \propto \int_{q_{min}}^{q_{max}} \int_{q_{min}}^{q_{max}} I(q_x, q_y) dq_x dq_y \quad (8)$$

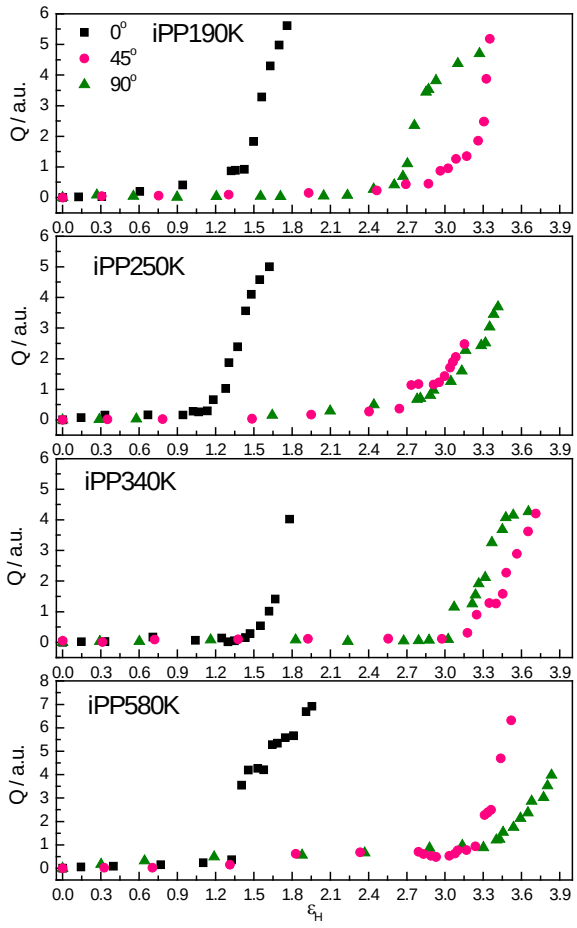

Fig. 5 The overall USAXS patterns integrated intensity as a function of strain for pre-oriented iPP samples stretched at 115 °C.

where $C_{e,c}$ and $C_{e,m}$ denote the average electron density distribution of cavities and the iPP matrix in the system, and ϕ_c refers to the volume fraction of cavities in iPP sample, respectively.

In Fig. 5, these total intensity values of *Q* were 0 at the early deformation stages and remained so until larger strains were imposed. Values of *Q* increased rapidly at certain strains where stress whitening began to be detected by USAXS technique. The gradual increase of *Q* with increasing strain is due to more and more cavities produced in the system. Clearly, such findings can be as a further evidence that cavitation activated at large strains causing stress whitening presented in all pre-oriented iPP samples during the second deformation process. Besides, the strain for *Q* beginning to increase in the 0° pre-oriented sample was always smaller than the ones in the other two pre-oriented ones for iPP with a certain molecular weight. This behavior will be discussed later. It must be mentioned that due to the arbitrary occurrence of the whitening within the sample during stretching and a small fixed location of X-ray beam the detection of cavitation scattering in USAXS experiments can be delayed compared to visual inspections as shown in Fig. 2.

The selected WAXS patterns of pre-oriented iPP580K during stretching at 115 °C, chosen as an example to illustrate the deformation behaviors at atomic length scale, are presented in Fig. 6. From these patterns, one can notice that the well-developed oriented structures were brought out in iPP580K after it was processed by die drawing procedure at 140 °C. During the second stretching, these pre-oriented molecular chains gradually changed to the new deformation direction and finally formed the same direction alignment structures. Interestingly, the stress whitening at large strains started to be activated only after the orientation direction of molecular chains was parallel to the new deformation direction, as reflected by the red circles which represent the strains just before initial stress whitening. Apart from that, only characteristic scattering peaks of α phase could be captured in WAXS patterns during the whole stretching process, meaning non-existence of other crystal modification. It should be emphasized that there were still some chains aligned perpendicular to the first deformation direction at strains of 0, even though these iPP samples had been stretched to a significant draw ratio by die drawing. We speculated this phenomenon resulted from the original crystallites with normal vertical to the die drawing direction. Because the draw ratio R_A of our die drawn iPP samples was only 2.27 which was not large enough for inducing perfect orientation of molecular chains in die drawn iPP, it was therefore possible to preserve a small amount of original crystallites.

Furthermore, the iPP with α phase is well famous for the cross-hatched structure (parent-daughter lamellae), which could be easily distinguished in the oriented sample based on the reflection from $(110)_\alpha$.[47, 48] The parent and daughter lamellae are normally 80° or 100° apart.[49] In Fig. 6, one could observe the reflections from daughter lamellae at the beginning deformation (e.g., the horizontal arcs on the $(110)_\alpha$ layer in 0° pre-oriented iPP), however, these scattering arcs disappeared at large strains due to stress-induced melting and recrystallization. All the molecular chains finally oriented along the deformation direction to form new crystallites. Besides, one could also find that the strains at which daughter lamellae disappeared were smaller than the strains triggering whitening at large strains for all samples. It indicates that the occurrence of branched lamellae had no influence on the initiation of whitening at large strains.

Fig. 7 collected the orientation parameters of crystallographic $(110)_\alpha$ plane as a function of strains and stresses according to equations 4, 5 and 6 using WAXS patterns shown in Fig. 6. The horizontal direction (the stretching direction) was selected as the reference direction during uniaxial stretching process. We first chose the 0° pre-oriented iPP580K to give an explanation of the relationship between chains orientation and strains. It can be seen the orientation degree of iPP580K was located at -0.2 after being processed by die drawing. That orientation degree continued to increase during the second deformation process and an orientation degree no less than -0.35 was required for stress whitening. For the other two pre-oriented directions samples, the initial orientation parameters were obviously above 0. As being mentioned before, for a perfect orientation of the lattice plane with its normal in the plane of equator, the order parameter *S* is equal to -0.5. If the lattice plane with its normal perpendicular to deformation direction, the perfect order parameter *S* is normally presented as 1. For the 90° pre-oriented iPP580K, the situation of chains orientation was more close to the latter case since the horizontal direction

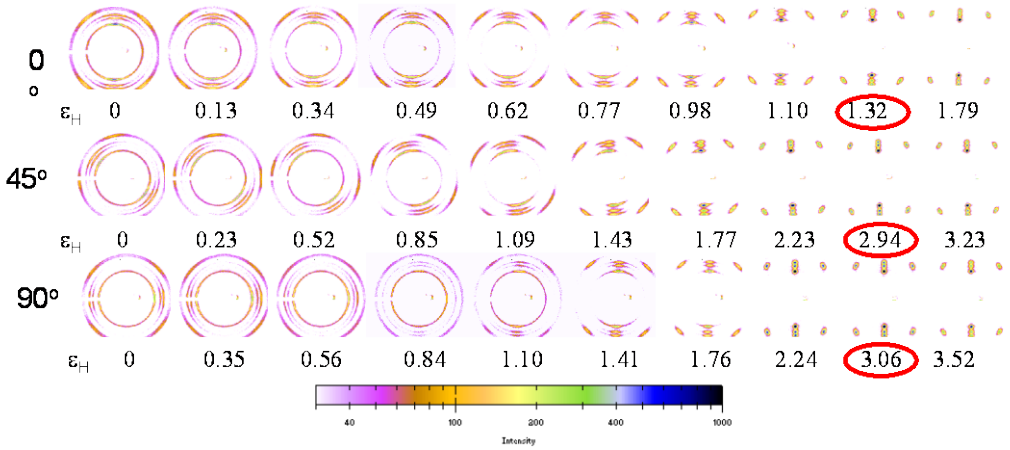

Fig. 6 Selected WAXS patterns of pre-oriented iPP580K samples drawn at 115 °C. The strains before initial stress whitening were marked by red circles. (The stretching direction is horizontal)

is defined as reference direction, thus, an orientation degree above 0 was observed in the 90° pre-oriented sample before the second deformation stage. In the case of the 45° pre-oriented one, the orientation direction of molecular chains was between the 0° and 90° pre-oriented iPP580K samples so that an intermediate value of orientation parameter was found at the initial state of the second stretching process. Nevertheless, the molecular chains of 45° and 90° pre-oriented iPP580K samples elongated along new deformation direction step by step during the second stretching. Therefore, the molecular chains of all these three iPP580K samples with different pre-orientation directions aligned along the same direction at the late stage of second stretching. Meanwhile, it also can be deduced that the stress whitening can only be triggered in highly oriented amorphous network oriented along the deformation direction.

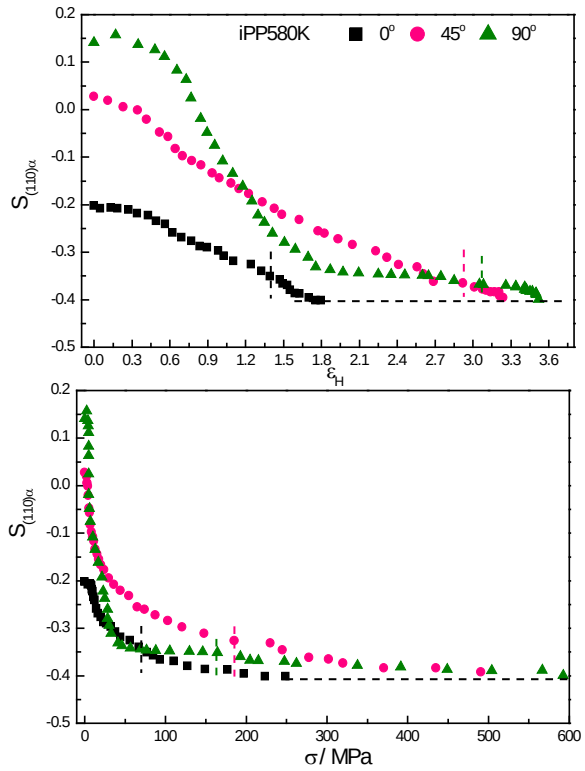

Fig. 7 Orientation parameters of crystallographic $(110)_\alpha$ plane of pre-oriented iPP580K samples stretched at 115 °C as a function of strains (top) and of stresses (bottom). The strains and stresses before initial stress whitening were marked by vertical dash lines.

Due to the origin of stress whitening activated at large strains being originated from the cavitation caused by the fragmentation of the inter-fibrillar tie chains,[30] the basic condition for such behavior is that of stretching fibrils to their limited extension.[30] Upon stretching, slippage of fibrils past each other led to further elongation of the already highly stretched entangled network. Such slippage is limited by the inter-fibril connections which are mainly entangled chains and tie molecules connecting adjacent fibrils. The entangled chains and tie chains can be broken and disentangled upon further stretching creating nucleation sites for the development of cavities. Obviously, for the 45° and 90° pre-oriented iPP samples, the molecular chains needed to be stretched to the state that chains oriented along the new deformation direction before the appearance of stress whitening at large strains. For attaining such high orientation degree, the 0° pre-oriented iPP580K sample clearly needed the smallest strain and stress while the 45° and 95° pre-oriented iPP580K sample required the larger strains and stresses according to results shown in Fig. 7. As a consequence, these latter two samples needed larger stresses to triggering stress whitening at large strains. That is also the reason for the smallest strain required in the 0° pre-oriented iPP samples for increasing *Q* in Fig. 5. However, for the different critical stresses of whitening presented in the 45° and 90° pre-oriented iPP samples, a deep understanding should be provided.

Fig. 8 depicts the selected SAXS patterns of pre-oriented iPP580K during stretching at 115 °C before stress whitening. The variation tendency of such patterns was similar to the trend observed in WAXS patterns in Fig. 6. At the beginning, the two slight scattering spots (e.g., the vertical scattering points in the 0° pre-oriented iPP) perpendicular to the two intensive scattering spots (e.g., the horizontal scattering points in the 0° pre-oriented iPP) were attributed by the unmelted original crystallites after die drawing. The fraction of these crystallites was about 29.4 % in the iPP580K system according to the method provided in the ESI of Fig. S2. During the second deformation process, the initial crystallites were destroyed

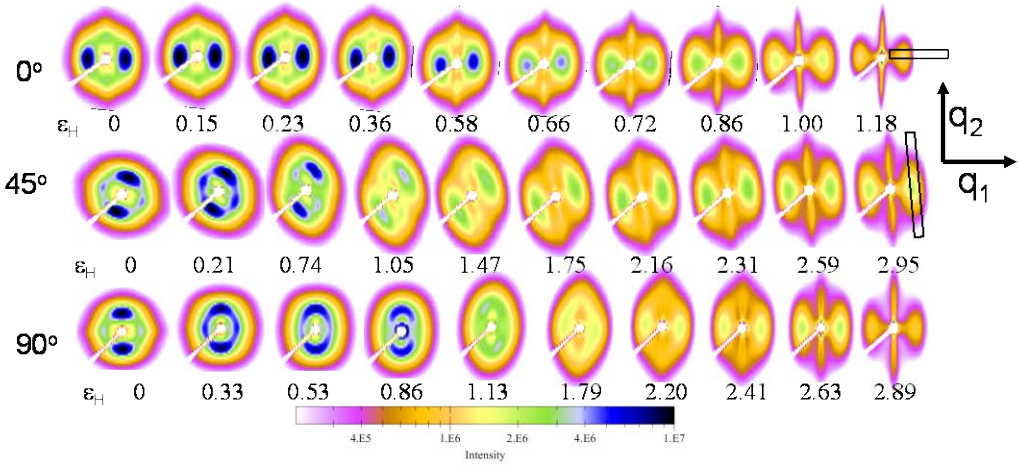

Fig. 8 Selected SAXS patterns of pre-oriented iPP580K samples drawn at 115 °C. (The stretching direction is horizontal)

(mechanical molten) and recrystallized to the new crystallites as proven by the two scattering spots along the deformation direction at large strains in all pre-oriented direction iPPs. In addition, one can observe the equatorial streaks across the beam spot in all samples at the late deformation stage, these equatorial streaks indicate the existence of micro-fibrils.[50-52]

In an effort to give a detailed description of the evolution of lamellae long spacing d_{ac} and lateral size l_{saxs}, the scattering vectors parallel and perpendicular to the normal direction of lamellae defined as q_1 and q_2 were employed to express this information, respectively. The rectangles displayed in Fig. 8 represent the integrating area for obtaining the respective one dimensional SAXS curves describing scattering intensity distributions along q_1 (from meridional direction) and q_2 (from equatorial one). The d_{ac} can be obtained according to equation 7. The corresponding results were summarized in Fig. 9. Even if the d_{ac} exhibited a slight dependency of iPP molecular weight at the beginning of the tensile process, the final d_{ac} values were basically the same irrespective of iPP molecular weight and pre-orientation direction of molecular chains, indicating all iPP samples developed the same thickness lamellae in the new tensile processes. Such performance is a typical feature of melting and recrystallization governing tensile deformation mechanism.[53] For the distinct d_{ac} presented in the different molecular weight iPPs after die drawing process, this was attributed to the incomplete melting of the original crystallites during die drawing.

In the case of the lateral size of lamellae l_{saxs}, the results are exhibited in Fig. 10. These data are calculated using the following function[54]

$$l_{saxs} = \frac{2\pi}{\Delta q_2} \quad (9)$$

the curves of I (q_2) were fitted with one Lorentz function, where Δq_2 describes the full width at half maximum of the Lorentz function fitting peaks. One thing should be mentioned here, the fitting profiles showed tiny deviation from their original curves, thus, the calculated l_{saxs} were relative rather than absolute values. However, such relative values do not affect the judgment of the tendency of l_{saxs} developed in all iPP samples during the second deformation process. Therefore, we can still use the corresponding results to analyze the evolution of the lateral size of new lamellae. Furthermore, the micro-fibrils are built up by stacks of crystalline lamellae whose normal are parallel to the stretching direction,[55] and thus the l_{saxs} can be considered as a reference for describing the width of micro-fibrils.[54]

As found in Fig. 10, the 45° and 90° pre-oriented iPP samples possessed a much smaller value of l_{saxs} than the 0° pre-oriented one. It can be deduced that the 0° pre-oriented iPP had micro-fibrils/fibrils with larger width than the systems of 45° and 90° pre-oriented ones for a certain molecular weight iPP after second stage tensile stretching. Thus, on a scale from the same cross sectional-area of fibrils, the number of load bearing inter-fibrillar tie chains in the 0° pre-oriented iPP samples formed during the second stretching was smaller than the ones in the 45° and 90° pre-oriented iPPs. Hence, a smaller stress was needed for breaking the oriented amorphous network composed of less number of load bearing inter-fibrillar tie

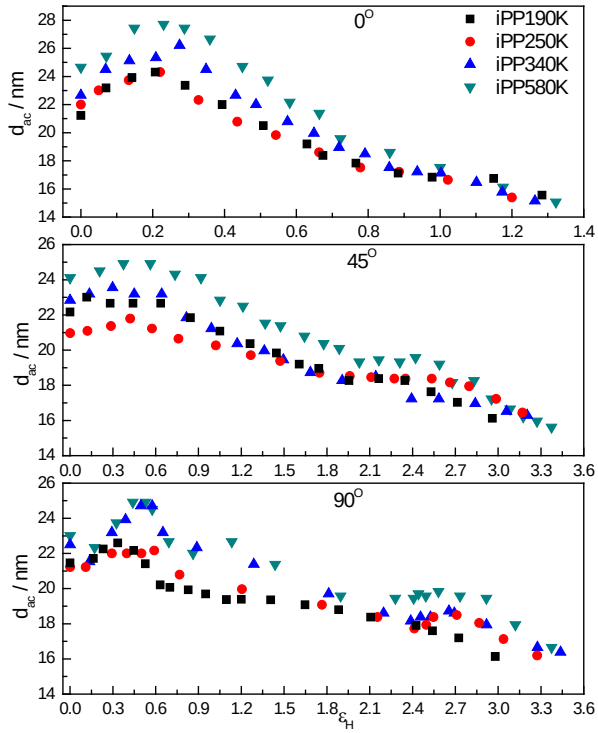

Fig. 9 The long space dac as a function of strains pre-oriented iPP samples deformed at 115 °C.

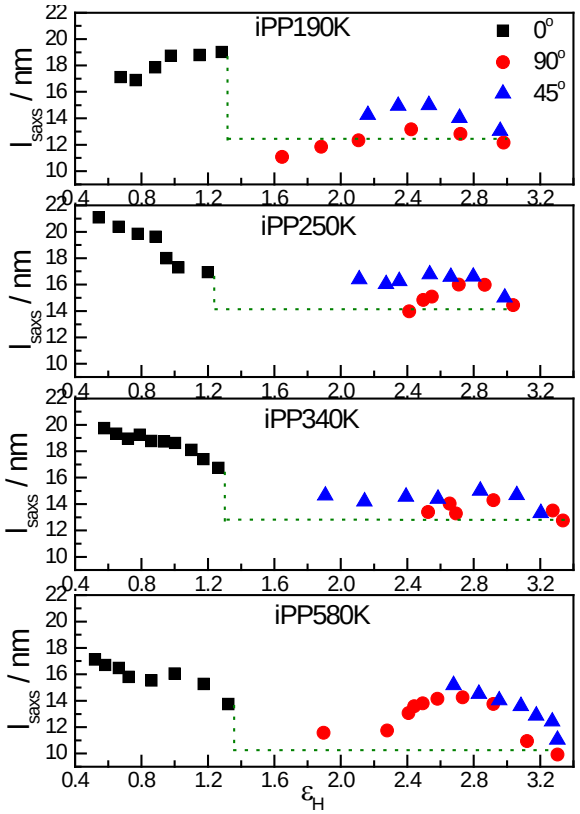

Fig. 10 The lateral size of lamellae as function of macroscopic strains of pre-oriented iPP samples deformed at 115 °C.

chains in the 0° pre-oriented iPP, and therefore leading to a lower critical stress of whitening at large strains. Moreover, the 45° and 90° pre-oriented iPP samples displayed the similar I_{saxs} while the different critical stresses of stress whitening were observed, manifesting that there was another potential factor which can influence the stress whitening behavior.

Fig. 11 gives the azimuthal integrated curves obtained along defined q_1 for illustrating the orientation process of micro-fibrils during the second deformation process. The insert SAXS pattern demonstrates the azimuthal integration area. As mentioned before, the scattering streaks close to the equatorial are originated from the micro-fibrils. Thus, the azimuthal peaks appeared around 90° in the integrated curves at the large strains belonged to the feature peaks of micro-fibrils, which are marked by green lines in the plot. Visibly, the variation of these peaks can be used to record the appearance and orientation degree of micro-fibrils upon stretching. For the 0° pre-oriented iPP, there was nearly no peak showed at the azimuthal angle of 90° but a sharp peak presented around the angle of 180° because its lamellae almost arranged at the meridional direction at the early tensile stage. With further stretching, this peak still kept its position at the azimuthal angle of 180° but two separated small peaks appeared at angles close to 90°. The latter two peaks were contributed by the micro-fibrils composed of the newly produced crystallites with their normal along the meridional direction.

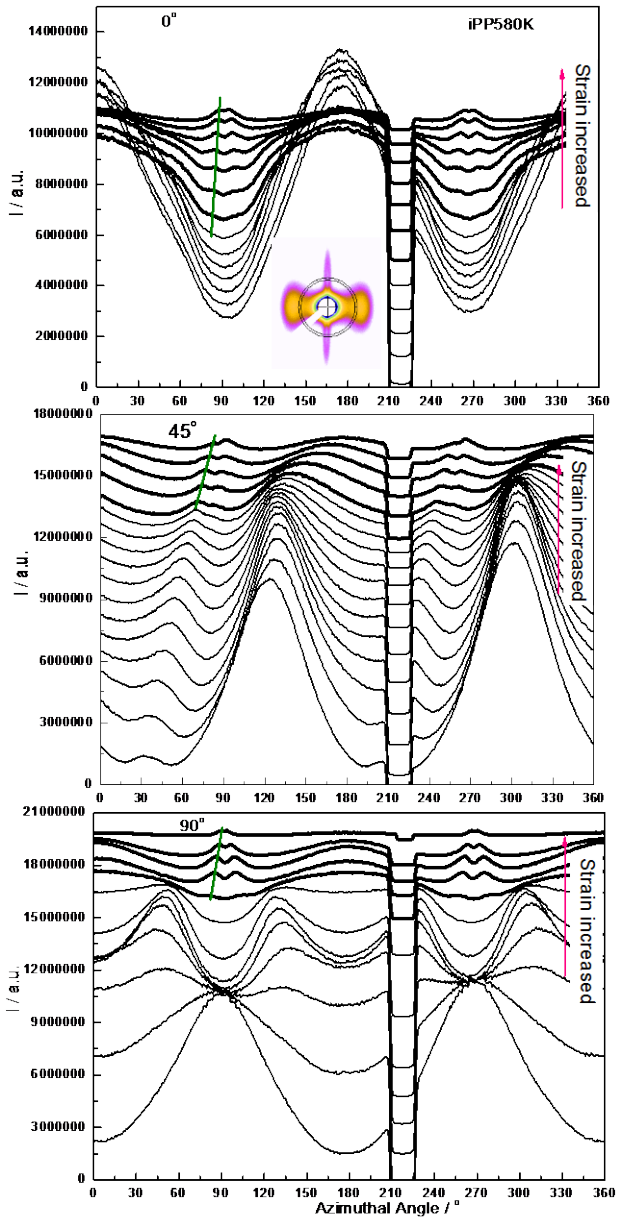

Fig. 11 The azimuthal integrated intensity of pre-oriented iPP580K samples at 115 °C taken at different strains. (The green lines marks the appearance and position of fibrils)

In the case of 90° pre-oriented iPP, a prominent peak around the azimuthal angle of 90° was observed before the second stretching, which were ascribed to the primary oriented lamellae with its normal along equatorial direction. Then, two distinct peaks occurred around the azimuthal angles of 45 and 135° when the stretching started, indicating pre-oriented crystallites began to slip and rotate. After entire destruction (mechanical melting) of these original crystallites, the stress-induced recrystallized lamellae appeared and arranged along the meridional direction. Thus, one peak at the azimuthal angle of 180° denoting the new crystallites and two peaks close to the angle of 90° devoted by micro-fibrils were observed at large strains. For the 45° pre-oriented iPP, the main oriented lamellae were located at 135° and 315° in the azimuthal integrated curves before stretching. These crystallites can be melted and finally recrystallized with their normal along the meridional direction, which also gave the same presentation as shown in the other two pre-oriented samples at late deformation stage. In summary, the two peaks around the azimuthal angle of 90° representing the typical position of micro-fibrils can be found in all pre-oriented iPP samples when the new crystallites were developed during second tensile deformation. The micro-fibrils usually occurred at the late deformation stage and then gradually oriented along the deformation direction.

For the purpose of comparing the relationship between the orientation degree of micro-fibrils and stress in different pre-oriented iPP samples during the second deformation, the corresponding results are presented in Fig. 12. Here, the analysis will be only given on the pre-orientation direction dependency of the orientation degree of micro-fibrils since all iPPs with different molecular weights showed the similar results. The black arrows represent the first appearance of micro-fibril peaks at equatorial region. Only a small stress was needed for the 0° pre-oriented iPP samples for inducing micro-fibrils while the 45° pre-oriented one visibly claimed the largest stress for the same movement in the current work. More importantly, an identified deviation of micro-fibril peaks from the azimuthal angle 90° still existed in the 45° pre-oriented iPPs although they were stretched to the high stress level. In the case of the 90° pre-oriented iPPs, their micro-fibrils could eventually locate at the azimuthal angle of 90°, meaning that a perfect orientation along deformation direction was achieved. However, these samples demanded a larger stress for the occurrence of micro-fibrils as compared to the 0° pre-oriented ones.

Combing the information from WAXS, SAXS and USAXS, we can finally propose the deformation models. The model

schemed in Fig. 13 is used to explain the possible mechanism of cavitation generated at large strains in the pre-oriented iPPs with different pre-orientation directions upon stretching. The detailed explanation of molecular weight dependency of cavitation activated at large strain in iPPs can be traced in our previous work.[30] As being confirmed, the mechanism of stress whitening at large strains of iPP is caused by the fragmentation of load bearing inter-fibrillar tie chains in highly oriented amorphous network.[30] The precondition for triggering such process is to enter the largest extension stage of fibrils. Then, the breakage of inter-fibrillar tie chains become rational by further stretching such fibrils in their limit state. On the basis of this opinion, it can be speculated that a near perfect alignment of fibrils with axes parallel to the deformation direction was the essential condition for inducing stress whitening at large strains in the pre-oriented samples during the second tensile process. Therefore, two stages for triggering stress whitening at large strains of pre-oriented iPP samples during the second deformation process were established.

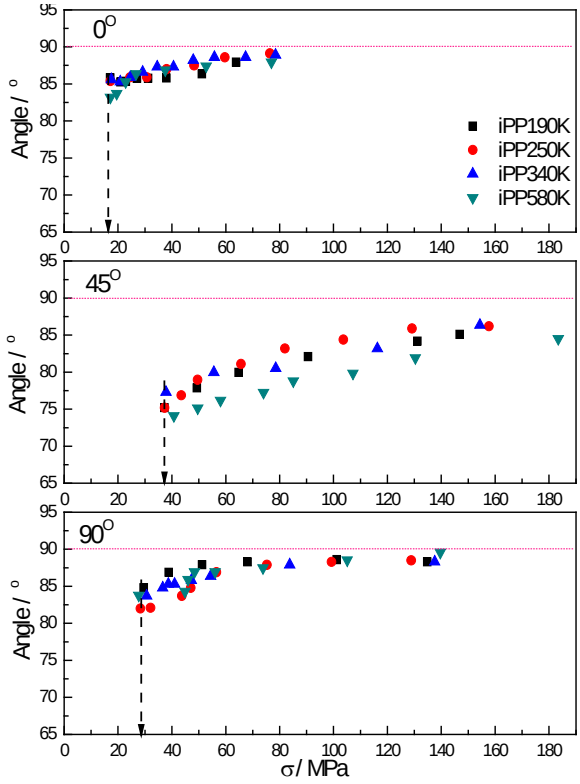

Fig. 12 The azimuthal position of microfibrils as a function of stresses of pre-oriented iPP samples during deformation process at 115 °C.

In the stage I, new crystallites formed with their normal along deformation direction, together with the development of micro-fibrils/fibrils with axes parallel to the deformation direction. Stage II started with further stretching of the newly-born micro-fibrils/fibrils, and then breakage of inter-fibrillar/micro-fibrils tie chains in this highly oriented amorphous network occurred due to the limited extension of fibrils/micro-fibrils which initiated the cavities simultaneously. Finally, the full-scale fragmentation of highly oriented amorphous network occurred because of the generation and growth of cavities in the whole system. Thus, a macroscopic fracture of materials was observed soon after the stress whitening triggered at large strains.

According to the lateral size of lamellae l_{saxs} shown in Fig. 10, the 0° pre-oriented iPP possessed the largest diameter of fibrils and the minimum number of inter-fibrillar tie chains for a certain molecular weight iPP on a scale from the same cross sectional-area of fibrils. Thus, the critical stress σ_h for destroying that oriented amorphous network in the 0° pre-oriented system was the smallest one as displayed in Fig. 13. For the 45 and 90° pre-oriented ones, their lateral sizes of lamellae l_{saxs} were smaller than the one in the 0° pre-oriented iPP, which means a highly oriented amorphous network with a larger number of inter-fibrillar tie chains could be achieved in these systems on a

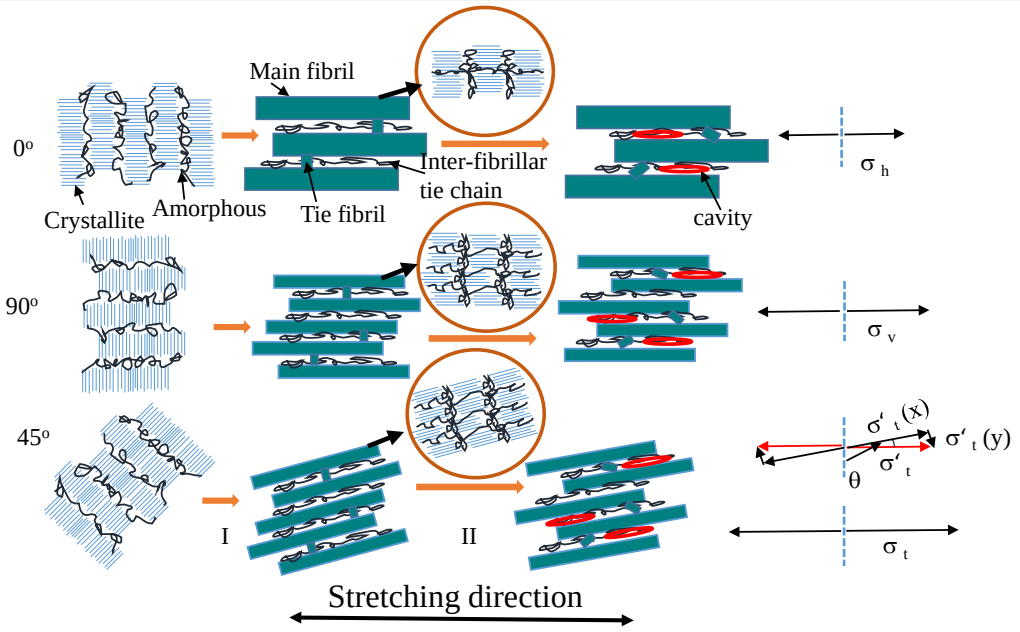

Fig. 13 Schematic presentation of the formation of cavities in fibrillar network of pre-oriented iPP with different pre-orientation directions. (Size not to scale)

scale from the same cross sectional-area of fibrils. As a consequence, a larger value of stress was required for damaging oriented amorphous networks in these samples. Obviously, we could expect the similar critical stresses of whitening at large strains in the 45 and 90° pre-oriented iPPs. However, our experimental results did not follow this hypothesis. Such behaviors may be attributed to the different orientation degrees of fibrils. Although the direct measurement of orientation of fibrils in pre-oriented iPP samples during second stretching was not possible in the current work, their variation can be reflected using the orientation of micro-fibrils as presented in Fig. 12. Before the fragmentation of oriented amorphous network, the fibrils in the 90° pre-oriented iPP had oriented along the deformation direction while the orientation of fibrils in the 45° pre-oriented one still showed a deviation from tensile direction.

Here, we considered that the states of oriented amorphous network in the 90° and 45° pre-oriented iPP samples were the same but only differed in the orientation degree during the second stretching. We use σ_v and σ_t' denoting the theoretical critical stress of whitening in the 90° and 45° pre-oriented iPPs, respectively. If the same tensile stress acted upon these two systems along fibril axis direction, we could observe the same critical stresses for activating stress whitening at large strains in the 90° and 45° pre-oriented iPP samples. However, the actual situation for the 45° pre-oriented one was that the tensile stress was not absolutely along the fibril axis direction. In other words, the direction of σ_t' was along the deformation direction not the fibril axis direction in the 45° pre-oriented iPP. In that case, σ_t' could not describe the actual critical stress of whitening in the 45° pre-oriented system. Thus, the stress of σ_t' needed to be orthogonally decomposed into two stress components. One is along the fibril axis direction ($\sigma_t'(x)$) and the other is vertical to the fibril axis direction ($\sigma_t'(y)$). Clearly, σ_t' (x) was the effective stress conducting the fragmentation of oriented amorphous network, which was smaller than the σ_t' and could not lead to the breakage of inter-fibrillar tie chains. It can be envisaged that the same value of σ_t' along the fibrils oriented direction (the direction of $\sigma_t'(x)$) was needed for supporting the destruction process. That means that a larger stress along the deformation direction was required in the 45° pre-oriented case. Moreover, the stress σ_t' (y) played a role to compress two adjacent fibrils together and prevent them slipping away from each other, then, an extra force was needed to be considered to balance this influence. Therefore, a further increment of stress σ_t along the deformation direction was necessary for breaking inter-fibrillar tie chains in the 45° pre-oriented iPP samples. On the macroscopic view, the largest critical stress of whitening was observed in that pre-oriented iPP sample in the present work. The function of σ_t' (y) was supposed to prevent the separation of two adjacent fibrils rather than promoting the departure due to the shrinkage of material in the equatorial direction, observed macroscopically. That behavior suggested the microstructures in the materials were normally squeezed along the direction vertical to the deformation direction.

4 Conclusions

The mechanism of stress whitening triggered at large strains in pre-oriented iPP samples prepared by die drawing process, was analyzed with respect to the iPP molecular weight and the previous orientation direction. For a certain pre-orientation direction, the critical stresses of whitening at large strains presented distinct differences in iPP samples with different molecular weights. Such behaviors were in accordance with our previous work and could also be as a further evidence that the stress whitening activated at large strains was associated with the fragmentation of inter-fibrillar tie chains in highly oriented amorphous network. More importantly, in this work we found that the critical stresses of whitening at large strains were related to the pre-orientation direction of molecular chains. The 0° pre-oriented iPP sample demanded the smallest critical stress of whitening at large strains but the 45° pre-oriented one required the largest critical value in the current work. The 0° pre-oriented iPP generally formed the oriented amorphous network containing the fibrils/micro-fibrils with larger diameter, whereas, the 45° and 90° pre-oriented iPPs developed oriented amorphous network embedded with fibrils/micro-fibrils which were much smaller in diameter. The morphologies of these oriented amorphous networks indicated that a smaller number of load bearing inter-fibrillar tie chains can be obtained in the 0° pre-oriented iPPs than the other two pre-oriented ones on a scale from the same cross sectional-area. Therefore, a lower critical stress was required for breaking oriented amorphous network of the 0° pre-oriented iPP system. For the 45° pre-oriented iPP, there existed a deviation angle between fibrils/micro-fibrils axis and the deformation direction. Compared to the 90° pre-oriented one, a much larger stress along deformation direction was needed in the 45° pre-oriented one, for providing effective critical stress parallel and extra stress vertical to the fibril axis to destroy oriented amorphous network and offset the stress preventing the separation of adjacent fibrils/micro-fibrils, respectively. Hence, the largest critical stress of whitening at large strains was observed in the 45° pre-oriented iPP samples in this work. Moreover, the macroscopic fracture of iPP always followed stress whitening at larger strains due to the full-scale breakage of the oriented amorphous network.

Conflicts of interest

There are no conflicts to declare.

Acknowledgements

This work is supported by the National Natural Science Foundation of China (21704102, 51525305, 21134006) and Royal Society (Newton Advanced Fellowship NA150222). We thank Dr. Tian Feng of SSRF for assistance during SAXS experiments and Dr. Ran Chen in our group for providing computer code to deal with WAXS, SAXS and USAXS data.

References

1 J. Xu, V. Mittal and F. S. Bates, *Macromolecules*, 2016, **49**, 6497-6506.
2 M. R. Mani, R. Chellaswamy, Y. N. Marathe and V. K. Pillai, *Macromolecules*, 2016, **49**, 2197-2205.
3 B. Zhang, B. H. Wang, J. J. Chen, C. Y. Shen, R. Reiter, J. B. Chen and G. Reiter, *Macromolecules*, 2016, **49**, 5145-5151.
4 Y.-H. Chen, G.-J. Zhong, Y. Wang, Z.-M. Li and L. Li, *Macromolecules*, 2009, **42**, 4343-4348.
5 R. H. Somani, B. S. Hsiao, A. Nogales, H. Fruitwala, S. Srinivas and A. H. Tsou, *Macromolecules*, 2001, **34**, 5902-5909.
6 H. Huo, S. C. Jiang, L. J. An and J. C. Feng, *Macromolecules*, 2004, **37**, 2478-2483.
7 J. C. Zhao, Z. G. Wang, Y. H. Niu, B. S. Hsiao and S. Piccarolo, *J. Phys. Chem. B*, 2012, **116**, 147-153.
8 J. Qiu, Z. G. Wang, L. Yang, J. C. Zhao, Y. H. Niu and B. S. Hsiao, *Polymer*, 2007, **48**, 6934-6947.
9 Q. Zia, H. J. Radusch and R. Androsch, *Polym. Bull.*, 2009, **63**, 755-771.
10 L. L. Fu, Z. Y. Jiang, H. F. Enderle, D. Lilge, Z. H. Wu, S. S. Funari and Y. F. Men, *J. Polym. Sci., Part B: Polym. Phys.*, 2014, **52**, 716-726.
11 Y. P. Liu, Z. H. Hong, L. G. Bai, N. Tian, Z. Ma, X. Y. Li, L. Chen, B. S. Hsiao and L. Li, *J. Mater. Sci.*, 2014, **49**, 3016-3024.
12 R. H. Somani, B. S. Hsiao, A. Nogales, S. Srinivas, A. H. Tsou, I. Sics, F. J. Balta-Calleja and T. A. Ezquerra, *Macromolecules*, 2000, **33**, 9385-9394.
13 H. N. An, B. J. Zhao, Z. Ma, C. G. Shao, X. Wang, Y. P. Fang, L. B. Li and Z. M. Li, *Macromolecules*, 2007, **40**, 4740-4743.
14 L. B. Li and W. H. de Jeu, *Macromolecules*, 2003, **36**, 4862-4867.
15 F. M. Su, W. M. Zhou, X. Y. Li, Y. X. Ji, K. P. Cui, Z. M. Qi and L. B. Li, *Macromolecules*, 2014, **47**, 4408-4416.
16 Z. G. Zhao, Q. Yang, M. Q. Kong, D. H. Tang, Q. Y. Chen, Y. Liu, F. L. Lou, Y. J. Huang and X. Liao, *Rsc Adv.*, 2015, **5**, 43571-43580.
17 N. Li, W. Cheng, K. Ren, F. Luo, K. Wang and Q. Fu, *Chinese J. Polym. Sci.*, 2013, **31**, 98-109.
18 K. Wang, M. Guo, S. Liang, P. Zhao, H. Yang, Q. Zhang, R. N. Du and Q. Fu, *Chinese J. Polym. Sci.*, 2007, **25**, 23-33.
19 Z. Y. Jiang, Y. T. Wang, L. L. Fu, B. Whiteside, J. Wyborn, K. Norris, Z. H. Wu, P. Coates and Y. F. Men, *Macromolecules*, 2013, **46**, 6981-6990.
20 K. Cui, L. Meng, N. Tian, W. Zhou, Y. Liu, Z. Wang, J. He and L. Li, *Macromolecules*, 2012, **45**, 5477-5486.
21 C. E. Chaffey, A. K. Taraiya and I. M. Ward, *Polym. Eng. Sci.*, 1997, **37**, 1774-1784.
22 A. K. Taraiya, M. S. Mirza, J. Mohanraj, D. C. Barton and I. M. Ward, *J. Appl. Polym. Sci.*, 2003, **88**, 1268-1278.
23 P. D. Coates, P. Caton-Rose, I. M. Ward and G. Thompson, *Sci. China Chem.*, 2013, **56**, 1017-1028.
24 P. D. Coates and I. M. Ward, *Polym. Eng. Sci.*, 1981, **21**, 612-618.
25 J. Mohanraj, N. Chapleau, A. Ajji, R. A. Duckett and I. M. Ward, *J. Appl. Polym. Sci.*, 2003, **88**, 1336-1345.
26 P. D. Coates and I. M. Ward, *Polymer*, 1979, **20**, 1553-1560.
27 A. Selwood, B. Parsons, I. M. Ward and A. Gray, *Plast. Rub. Proc. Appl.*, 1989, **11**, 229-233.
28 A. G. Gibson and I. M. Ward, *Polym. Eng. Sci.*, 1980, **20**, 1229-1235.
29 I. M. Ward, *Angew Makromol. Chem.*, 1982, **109**, 25-39.
30 Y. Lu, Y. T. Wang, R. Chen, J. Y. Zhao, Z. Y. Jiang and Y. F. Men, *Macromolecules*, 2015, **48**, 5799-5806.
31 Y. T. Wang, Z. Y. Jiang, L. L. Fu, Y. Lu and Y. F. Men, *Plos One*, 2014, **9**, e97234.
32 Y. F. Men, J. Rieger and J. Homeyer, *Macromolecules*, 2004, **37**, 9481-9488.
33 A. Galeski and A. Rozanski, *Macromol Symp*, 2010, **298**, 1-9.
34 S. Humbert, O. Lame, J. M. Chenal, C. Rochas and G. Vigier, *Macromolecules*, 2010, **43**, 7212-7221.
35 I. C. Yeh, J. L. Lenhart, G. C. Rutledge and J. W. Andzelm, *Macromolecules*, 2017, **50**, 1700-1712.
36 A. Rozanski, A. Galeski and M. Debowska, *Macromolecules*, 2011, **44**, 20-28.
37 R. Chen, Y. Lu, J. Y. Zhao, Z. Y. Jiang and Y. F. Men, *J. Polym. Sci., Part B: Polym. Phys.*, 2016, **54**, 2007-2014.
38 R. Y. Bao, Z. T. Ding, G. J. Zhong, W. Yang, B. H. Xie and M. B. Yang, *Colloid Polym. Sci.*, 2012, **290**, 261-274.
39 Z. Cai, Y. Zhang, J. Li, F. Xue, Y. Shang, X. He, J. Feng, Z. Wu and S. Jiang, *Polymer*, 2012, **53**, 1593-1601.
40 R. H. Lv, W. F. Xu, B. Na, Q. Zhang and Q. Fu, *J. Polym. Sci., Part B: Polym. Phys.*, 2008, **46**, 1202-1206.
41 M. W. Ian, D. C. Phil and M. D. Michel, *Solid Phase Processing of Polymers*, Hanser, Munich, Germany, 2000.
42 P. Hermanns and P. Platzek, *Kolloid-Zeitschrifi*, 1939, **88**, 68-72.
43 M. Polanyi, *Z Phys*, 1921, **7**, 149-180.
44 A. K. Taraiya, A. Richardson and I. M. Ward, *J. Appl. Polym. Sci.*, 1987, **33**, 2559-2579.
45 F. Zuo, J. K. Keum, X. M. Chen, B. S. Hsiao, H. Y. Chen, S. Y. Lai, R. Wevers and J. Li, *Polymer*, 2007, **48**, 6867-6880.
46 G. Strobl, *The Physics of Polymers*, Springer, Berlin, Germany, 2nd edn., 1997.
47 L. Ma, J. Zhang, M. A. Memon, X. L. Sun, H. H. Li and S. K. Yan, *Polym Chem-Uk*, 2015, **6**, 7524-7532.
48 L. Ma, Z. Z. Zhou, J. Zhang, X. L. Sung, H. H. Li, J. M. Zhang and S. K. Yan, *Macromolecules*, 2017, **50**, 3582-3589.
49 B. Lotz, J. C. Wittmann and A. J. Lovinger, *Polymer*, 1996, **37**, 4979-4992.
50 I. Coccorullo, R. Pantani and G. Titomanlio, *Polymer*, 2003, **44**, 307-318.
51 Y. Lu, R. Chen, J. Zhao, Z. Y. Jiang and Y. F. Men, *J. Phys. Chem. B*, 2017, **121**, 6969-6978.
52 Y. M. Mao, X. W. Li, C. Burger, B. S. Hsiao, A. K. Mehta and A. H. Tsou, *Macromolecules*, 2012, **45**, 7061-7071.
53 Corneliu.R and A. Peterlin, *Makromolekul. Chem.*, 1967, **105**, 193-203.
54 Y. J. Tang, Z. Y. Jiang, Y. F. Men, L. J. An, H. F. Enderle, D. Lilge, S. V. Roth, R. Gehrke and J. Rieger, *Polymer*, 2007, **48**, 5125-5132.
55 A. Peterlin, *Colloid Polym. Sci.*, 1975, **253**, 809-823.